

# SeagrassFinder: Deep Learning for Eelgrass Detection and Coverage Estimation in the Wild

Jannik Elsässer  
DHI Group  
Hørsholm, Denmark  
jael@dhigroup.dk

Laura Weihl  
IT University of Copenhagen  
Copenhagen, Denmark  
lawe@itu.dk

Veronika Cheplygina  
IT University of Copenhagen  
Copenhagen, Denmark  
vech@itu.dk

Lisbeth Tangaa Nielsen  
DHI Group  
Hørsholm, Denmark  
litn@dhigroup.com

**Abstract**—Seagrass meadows play a crucial role in marine ecosystems, providing important services such as carbon sequestration, water quality improvement, and habitat provision. Monitoring the distribution and abundance of seagrass is essential for environmental impact assessments and conservation efforts. However, the current manual methods of analyzing underwater video transects to assess seagrass coverage are time-consuming and subjective. This work explores the use of deep learning models to automate the process of seagrass detection and coverage estimation from underwater video data. A dataset of over 8,300 annotated underwater images was created, and several deep learning architectures, including ResNet, InceptionNetV3, DenseNet, and Vision Transformer, were evaluated for the task of binary classification of “Eelgrass Present” and “Eelgrass Absent” images. The results demonstrate that deep learning models, particularly the Vision Transformer, can achieve high performance in predicting eelgrass presence, with AUROC scores exceeding 0.95 on the final test dataset. The use of transfer learning and the application of the Deep WaveNet underwater image enhancement model further improved the models’ capabilities. The proposed methodology allows for the efficient processing of large volumes of video data, enabling the acquisition of much more detailed information on seagrass distributions compared to current manual methods. This information is crucial for environmental impact assessments and monitoring programs, as seagrasses are important indicators of coastal ecosystem health. Overall, this project demonstrates the value that deep learning can bring to the field of marine ecology and environmental monitoring.

**Index Terms**—Deep Learning, Marine Biology, Marine Ecology, Marine Imaging, Computer Vision, Transfer Learning

## I. INTRODUCTION

Seagrasses are a type of marine flowering plant that are of fundamental importance in the health and integrity of coastal ocean habitats, biodiversity, global climate, human economic stability (Cullen-Unsworth et al., 2014) as well as global food security (Unsworth et al., 2019). Despite ongoing conservation efforts, seagrass meadows are declining globally at an alarming rate due to human activities and coastal development, and exacerbated further by climate change (Waycott et al., 2009). These factors collectively contribute a stark decline water quality and threaten the long-term survival of seagrass habitats. There is a growing interest in offshore infrastructure such as windfarms which offer a potential solution to the energy crisis but also raise concerns about environmental impacts. We need to effectively measure and quantify the impacts of these interventions to the local underwater environments.

Environmental Impact Assessments (EIAs) conducted by private companies are designed to oversee offshore building sites and their impacts to ensure environmental compliance with different stakeholders across the marine infrastructure sector. Monitoring is often conducted in form of video transects; a camera is mounted onto a sled and towed behind a vessel to capture underwater video footage. The resulting recorded videos are then meticulously annotated by marine biologists.

One crucial challenge here is data acquisition and repeated monitoring of the condition and distribution of such seagrass meadows in a structured, automated and efficient manner (Unsworth et al., 2019). Some automation approaches like remote sensing have shown success but fail to distinguish between different types of seagrass (Riegl and Purkis, 2005). Recently, there is growing interest in detecting and classifying seagrasses directly from underwater (UW) image or video data taken in the wild to gain more fine-grained knowledge on the health of seagrass meadows. Acquiring this visual data is very costly in terms of human efforts and operational investments as it requires expertise not only in technical equipment but also in marine biology. It is a priority to overcome these costs and challenges by automation, specifically by applying image analysis.

With the advent of deep learning, our capacity to analyze and process data has transformed significantly. Specifically deep neural networks (DNNs) have shown remarkable success in a wide range of computer vision tasks such as image classification, semantic segmentation and object detection. DNNs achieve this by learning information directly from raw pixel input data without the need for manual feature engineering. Especially convolutional neural networks (Krizhevsky et al., 2012) massively improved our ability to automatically extract relevant features and have become the new standard in computer vision tasks. Successfully training DNNs with high accuracy is dependent on the quality and quantity of input data, the training procedure and the type of DNN models used. The advantage here is that this allows for adaptation to a variety of image qualities and conditions (such as blurry, color-distorted or underexposed underwater images) as long as labeled samples are sufficiently present in the training set. However this also marks a challenge since DNNs require large amounts of such samples which in turn requires vast human annotation efforts.

The objective of this work is to address all above-mentioned limiting factors of training DNNs for seagrass detection in the

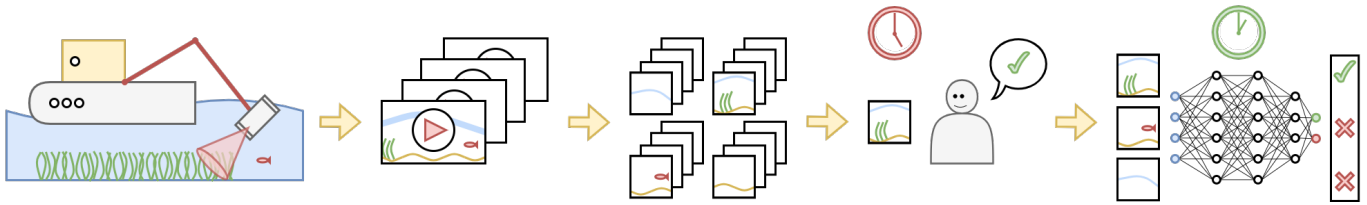


Fig. 1: The SeagrassFinder Project Pipeline: a vessel tows a sled with a camera along the seabed and records videos of the UW environment. The extracted images are labeled by human annotators and used to train a DNN on the task of detecting eelgrass. The trained DNN can now be used to replace the time-consuming manual annotation process.

wild by; (1) deploying an efficient image annotation platform to gather large amounts of labeled data (2) implementing an effective training procedure for our underwater video data set, (3) investigating a range of DNN models on their capacity to learn seagrass features via transfer learning. The data used in this project was taken from DHI’s Environmental Impact Assessment (EIA) and baseline reporting of the Lynetteholm project, a new artificial peninsula being created to extend the coastline of northern Copenhagen in Denmark.

We address the challenge of estimating seagrass presence and coverage in the wild from vast amounts of raw, unstructured and unfiltered video data taken in realistic environmental conditions. We achieve this by deploying a custom-made annotation platform for simplified manual labeling, as well as training state-of-the-art deep learning models with a specific focus on classifying whether eelgrass is present or absent in an image. Specifically we contribute the following:

- a strategy for effectively streamlining human labeling efforts of experts in the field as well as non-experts on underwater seagrass images and compiling the annotated data set into an efficient ML data pipeline,
- a novel annotated image data set of eelgrass under realistic non-artificial lighting conditions extracted from raw videos of underwater transect surveys in the wild <sup>1</sup>,
- an analysis of state-of-the-art DNN models and their ability to classify a range of challenging underwater images according to the presence eelgrass using a transfer learning mechanism, as well as an investigation of the effect of UW image enhancement on DNN performance,
- a new experimental approach for further utilizing above-mentioned DNN models for estimating visual eelgrass coverage for an image stream from binary predictions as a post-processing step,
- a pipeline for significantly reducing the time and financial resources required for human annotation tasks and paving the way towards potential automated environmental monitoring of seagrass for example by means of autonomous underwater vehicles.

To the best of our knowledge we are the first to deploy state-of-the art Vision Transformers to detect the presence of eelgrass in images in this line of research.

### A. Seagrass

Seagrasses are a type of submerged aquatic vegetation (SAV) found in shallow waters along every continent in the world except Antarctica (Novak and Short, 2020). Seagrass meadows are monitored worldwide as part of environmental impact assessments (EIAs) and environmental monitoring programs because they provide important ecosystem services, such as carbon sequestration, water quality improvement, providing food and habitat, and acting as a biological indicator of local ecosystems (Novak and Short, 2020). Seagrass meadows play a crucial role as a major carbon sink worldwide and are essential for mitigating the impacts of global climate change. Although seagrasses cover only 2% of the ocean’s seabed, they account for over 15% of the carbon annually sequestered in marine environments (Fourqurean et al., 2012). Besides their contributions to carbon sequestration and exportation, seagrass meadows also act as filters, enhancing water quality and clarity by directly capturing suspended particles and retaining organic matter (Terrados and Duarte, 2000). Seagrass meadows serve as vital hubs of biodiversity, offering nourishment and shelter to a wide range of organisms, including endangered species like dugongs and commercially significant ones such as fish and shrimp, alongside microbes and invertebrates (Fry and Parker, 1979). Furthermore, due to seagrasses significant vulnerability and rapid response to anthropogenic stressors such as eutrophication, sedimentation, oil spills and commercial fishing, seagrasses also act as biological indicators of coastal conditions (Orth et al., 2006).

Estimating the abundance of seagrass is critical to judging seagrasses ecosystem functions (Hemminga and Duarte, 2000). Multiple methods are used to determine seagrass abundance, all evaluating one or more of the following categories: seagrass leaf cover, biomass, shoot density and canopy height (Short and Coles, 2001). Transects are specifically used to determine seagrass abundance over a range of water depths (Short and Coles, 2001).

Determining the maximum water depth at which seagrass grows is critical during EIA and environmental monitoring programs. This metric can be used as a proxy for estimating any anthropogenic impact on the local marine ecosystem, of which impacts will be most significant to the maximum water depth at which seagrass grows.

There exist various species of seagrass, with *Zostera marina* or “eelgrass” being the specific seagrass species which is monitored as part of the Lynetteholm EIA, and therefore also

<sup>1</sup>DOI: zenodo.org/records/13904604

the species of seagrass which models in this report have been trained on. However, in the context of using computer vision, seagrasses' characteristic leaf morphology, density variations contributing to distinctive underwater meadow structures, and consistent color spectra suggest that methods applied to eelgrass can possibly work on other taxonomically similar species, and vice versa.

### B. Related Work

Multiple other studies have pursued similar efforts to automate eelgrass detection, classification and coverage estimation based on analysis of image data using various methods including DNNs. Prior work for seagrass coverage estimation includes segmenting images into superpixels and training a logistic regression classifier to distinguish image patches between seagrass and background (Reus et al., 2018). This method might not generalize well to images at different resolutions, scale of objects or water depths because of the fixed patch size constraint and the dependency on the quality of the superpixels. We propose a new approach based on estimating seagrass coverage efficiently from binary classifications in an image stream.

In *SeaGrassDetect* (Sengupta et al., 2020), the authors use unlabeled image data collected by a scuba diver towed by a boat to detect seagrass and estimate its coverage. They circumvent the necessity of labeled ground truth data by leveraging the structural characteristics of seagrass. They apply edge and line detection to extract the number of eelgrass stalks in an image and the total length of the lines which are combined with a weighted threshold strategy to infuse a Gaussian mixture model for binary classification. In our work we use an end-to-end seagrass detection approach where the entire image is fed into a DNN, removing the dependency on the sensitivity of feature engineering like line detection.

Previous studies incorporate the training of DNN models to detect a specific seagrass species called *Halophila ovalis* in images, captured in controlled lab environments with artificial lighting and real UW environments (Noman et al., 2023), (Moniruzzaman et al., 2019). Another line of research is to optimize DNNs for multi-species seagrass detection and classification (Raine et al., 2020) or for specific hardware constraints (Wang et al., 2020). We focus on the detection of a single seagrass species in the wild and investigate the performance of multiple DNN architectures on this task.

Other methods for seagrass monitoring include remote sensing (Veettil et al., 2020) collected from satellite images (Riegl and Purkis, 2005), aerial footage (Roelfsema et al., 2015), acoustic sensors (Gumusay et al., 2019), scuba divers (Sengupta et al., 2020) or remotely operated vehicles (Finkl and Makowski, 2016). However we focus on analyzing large amounts of unstructured video data gathered in the wild from EIA transect videos. This allows us to adhere to already established standard operating procedures for quality assurance in monitoring efforts as part of EIAs.



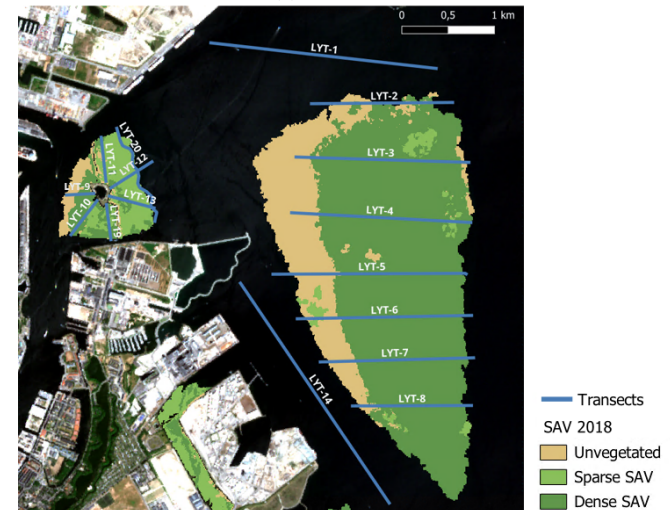
(a) Unvegetated



(b) Sparse SAV



(c) Dense SAV



(d) Transect Map

Fig. 2: (a) - (c) Sample images of areas with no, sparse and dense submerged aquatic vegetation (SAV). (d) A map of the Copenhagen harbor with transect lines (blue) and SAV data overlaid. All SAV maps are based on © Copernicus Sentinel-2 data from 2023-06-13. All SAV maps are based on analysis of Sentinel-2 imagery from 2018.

Transect Name	Length (km)	Water Depth (m)	Video Length (min)
LYT-5	2.00	5.5 → 12.4	20
LYT-9	0.29	2.7 → 7.4	5
LYT-10	0.45	3.0 → 6.0	10
LYT-12	0.50	3.4 → 12.8	10
LYT-14	3.00	13.8 → 14.1	60
LYT-20	1.20	9.5 → 9.6	45

TABLE I: Transect Details. All transects were filmed in June 2023 over two consecutive days during daytime.

## II. MATERIALS AND METHODS

### A. Data Acquisition

We gather a novel annotated image data set of *Zostera marina* from six EIA transect surveys in and outside the Copenhagen harbour, covering an area of roughly 10km<sup>2</sup>. In total we consider 20 survey transects over two consecutive days in June 2023 during daytime. Each survey produces a transect video of the local benthic environment. During an eelgrass transect survey, an underwater camera is mounted on a sled and towed behind the survey vessel along a planned route of interest. The sled ensures the camera maintains a consistent angle and prevents it from swinging in the water current. A technician or biologist on the vessel monitors the depth of the sled and monitors its height above the seafloor, adjusting its height to avoid obstacles or to perform necessary maintenance such as cleaning the camera lens. After the field data collection, a marine biologist reviews the camera footage and adds annotations to a spreadsheet. These annotations include timestamps, the vessel’s location, and any notable changes in eelgrass coverage or other observations. All videos are filmed with an underwater camera with a 1/3” 2 Mega pixel Sony CMOS sensor.

As part of the EIA of the Lynetteholm, project DHI performs 20 eelgrass video transects annually. Out of all 20 video transects of 2023 we choose a subset of six transect videos for their high degree in variability in visual content, i.e. changing seabed, as well as their roughly equal class distribution of eelgrass present vs. absent images. We estimate this based on earth observation data provided by DHI as part of the EIA, which showed SAV areas of interest (see Fig. 2d), and initial data inspection. Each selected transect video is between 5–60 minutes long and recorded at 30 FPS while the survey vessel sails at roughly 1m/s. We extract frames at 5 FPS from the survey videos in order to strike a balance between the volume of data and the informational content. This also ensures that consecutive frames are sufficiently distinct. In total we extracted 340,000 images from our selected transect videos. We crop all frames to 1280x500 pixels to remove any overlay information (see samples in Fig. 2). From each transect video we randomly sample images to create the dataset, resulting in total of 16,000 images.

### B. Data Annotation and Platform

With our data annotation platform SeagrassFinder, our goal is to create a streamlined annotation process to enable easy

access via a browser on any device of an annotator’s preferred choice. We considered using already existing annotation platforms however found that they did not provide a UI which was both easy to access and mobile friendly, and therefore developed our own. We named this app SeagrassFinder, to keep the URL of the app simple and memorable. In the context of the paper, we refer to the annotation platform as SeagrassFinder AP. SeagrassFinder AP is a Python Streamlit application deployed as an Azure App Service, connected with an Azure SQL Database for saving the annotations, with individual images hosted on an Azure Storage account. The aim is to create an intuitive and self-explanatory interface that enables a fast labeling process. Since we expect a relatively small count of distinct users we decide to only require users to enter their name without a user having to sign up for an account.

The interface of SeagrassFinder AP is designed to be straightforward with minimal amount of text to keep the barrier of entry for a new user as low as possible (see Fig. 3a). We also keep the explanation extremely brief and simplify the task instructions by adding visual guidance with concrete image examples with eelgrass present and absent. Alongside the two label buttons we add a button to skip the current sampled image as well as a button to undo the previous annotation. A user can also submit a comment if an image is considered invalid. For each annotation task we uniformly sample an image from the data set and display it to the annotator to maximise objectivity and to avoid showing consecutive frames which could potentially add labeling bias. To motivate users to annotate as many images as possible we add a leaderboard to the platform, to spark competitiveness between users which proved highly effective.

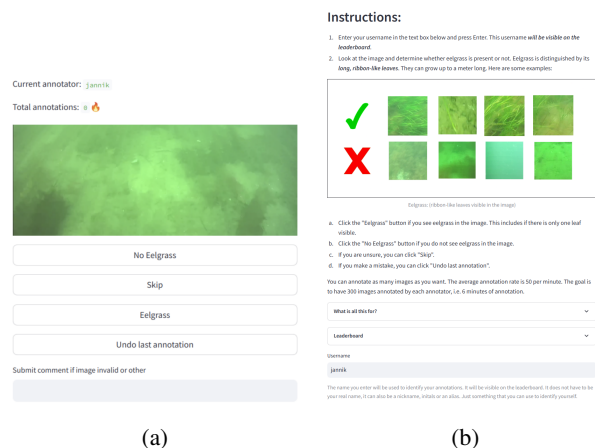


Fig. 3: (a) A screenshot of the SeagrassFinder Annotation Platform accessed through a browser window. The labeling interface is simple and intuitive. (b) A screenshot of the start page of the SeagrassFinder AP showing the visual guidance for the labeling instructions.

### C. Annotation Analysis

We conduct an analysis of the annotations collected via SeagrassFinder AP since their correctness has a direct



influence on the performance of our DNN model predictions. In total we have 19 different users creating more than 13000 annotations on more than 8900 different images. We calculate metrics to analyze the inter-annotator agreement level such as annotation agreement percentage, Cohen’s Kappa for reliability of annotators as well as mistake rate, i.e. rates of “mistake” and “ambiguous” annotations.

Generally, all annotators exhibit a high degree of annotation agreement, with annotators agreeing with one another on average 76% of the time. Very few annotators (3 out of 19) exhibit a lower than 70% agreement. We also investigate the impact of non-expert annotators annotating images and found that no bias is present between images annotated by non-expert annotators. There is also no connection between annotators with a lower agreement level, and their domain experience. This confirms that the classification of UW images for eelgrass presence is an annotation task humans are capable of, independent of annotators being experts or non-experts. This is still true for more challenging images with high levels of blur, color-distortion or low contrast.

We report how many times an image is labeled in Fig. 4a. Additionally we calculate the probability of agreement for each image normalized relative to the number of annotations (see Fig. 4b). For images that are annotated twice, the annotators achieve an overall 93% agreement. Cohen’s Kappa scores are calculated between every annotator’s subset of common annotated images and reported in the format of a matrix (see appendix Fig. 11). Using magnitude guidelines defined by Landis et al. (Landis, 1977) we find that on average there is a level of agreement is of *substantial* to *almost perfect* magnitude. In occasions where less than or moderate agreement is seen, we find that this is caused by a too small sample size of commonly annotated images.

To estimate the mistake rate of annotators we consider two types of disagreements in annotations which we verify manually; a “mistake annotation” where a user accidentally clicks the wrong label button caused by an obvious lapse in judgment by visual inspection, and an “ambiguous annotation” where eelgrass is only partially visible or eelgrass presence was uncertain. By labeling ambiguous annotations we estimate to which degree annotators make mistakes, and if the annotation task was not defined well enough. Based on the ratio of ambiguous to mistake annotations we dismiss the presumption that the annotation task was too vague. However it does highlight that the task of annotating can be at times very difficult to complete. Among the annotators, mistake annotations occur at a fairly low rate, on average at around 8% (see Fig. 12.) There seems to be no relation between the level of disagreement percentage of a user and their mistake percentage.

#### D. Final Dataset Compilation

A detailed overview of our data set strategy for the DNN training and testing pipeline can be seen in Tbl. II. First we manually remove all images taken above sea-level manually to mitigate inclusion of non-relevant features (this can be done quite quickly by trimming the video to once it is underwater).

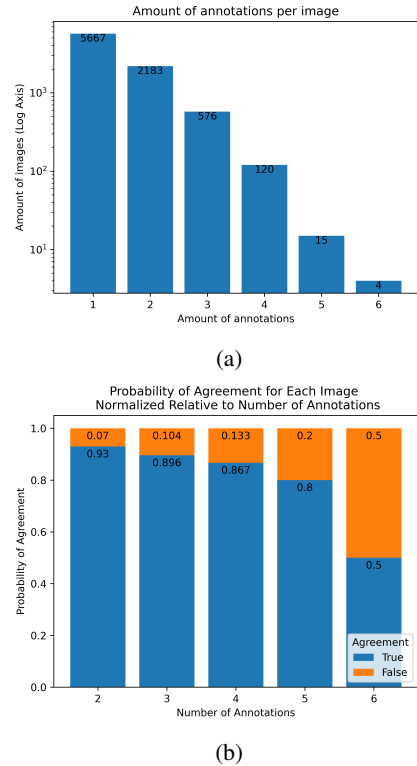


Fig. 4: (a) The number of images on log-scale vs. the number of times the image was annotated. (b) The probability of agreement for each number of annotations.

Additionally we filter out all images with disagreeing annotations. The final dataset consists of 8324 images, 52% of which are labeled as “Eelgrass Present”. To avoid data leakage between train and test set we do not mix images between different transects. Throughout the project, we hold out transect LYT-9 as the final test dataset. In all experiments we split the train data into validation sets of 20% using random split procedure.

#### E. Deep Learning Methodology

In this work, we adopt transfer learning to train a number of DNN models on the specific task of classifying images for two classes; “Eelgrass Present” and “Eelgrass Absent”. We analyse four different model architectures;

- ResNet (He et al., 2016): a convolutional architecture incorporating residual blocks to address the challenge vanishing/exploding gradients in DNN training,
- InceptionNetV3 (Szegedy et al., 2016), a convolutional architecture using multiple filter sizes to extract both local and global features, enhancing its capability to represent complex patterns in the input data,
- DenseNet (Huang et al., 2017), a convolutional architecture which uses a dense connectivity pattern, allowing for better information and gradient flow throughout the network,
- Vision Transformer (ViT) (Dosovitskiy, 2020), a state-of-the-art vision model which incorporates an attention

Transect Name	#Images	#Images Annotated	Eelgrass Present	Init. Train Dataset	Init. Test Dataset	Cross Val. Dataset	Final Train Dataset	Final Test Dataset
LYT-5	4000	2116	93.5%	✓			✓	
LYT-9	2000	1044	53.5%					✓
LYT-10	2000	1066	61.5%	✓		✓	✓	
LYT-12	2000	1069	52.2%	✓		✓	✓	
LYT-14	4000	2126	2.6%	✓			✓	
LYT-20	2000	1079	60.2%		✓	✓	✓	
<b>Total</b>	16000	8500	53.9%	6377	1079	3214	7456	1079

TABLE II: A summary of our data strategy: each transect results in a video from which we extract and annotate a subset of images. We show the percentage of images with eelgrass labels. We list the datasets used for initial hyperparameter tuning and cross validation (cross val.). We excluded LYT-5 and LYT-14 from cross validation because of their high class imbalance. LYT-9 was chosen as the final test set and therefore excluded from all other training/testing procedures. All remaining images were used in the final model training.

mechanism that overcomes inductive biases suffered from convolutional architectures.

All models are available online with pre-trained weights in PyTorch (Paszke et al., 2019), and are pre-trained on the ImageNet (Russakovsky et al., 2015) dataset. We fuse each model with two additional fully-connected layers for performing classification. During the training process, we only fine-tune the weights of the additional layers while the weights of each pre-trained model are frozen. A visualization of the transfer learning mechanism can be seen in Fig. 5. We evaluate the performance of our chosen DNN models according to three metrics:

- accuracy ( $\uparrow$ ): the percentage of correct predictions,
- area under receiver operating characteristic curve (AUROC or AUC) ( $\uparrow$ ): ability of a model to distinguish between classes across all possible classification thresholds,
- test calibration error (CE) (Kumar et al., 2019) ( $\downarrow$ ): the discrepancy between model predictions and the true probabilities given the model outputs. This is not a common metric for computer vision applications, however, it has been recently recommended for medical image analysis (Maier-Hein et al., 2024), a fine-grained classification task which shares properties with our data. CE scores range between 0 and 1, where  $CE = 0$  means the model is perfectly calibrated.

Throughout this document, where higher values mean better performance, metrics are marked with ( $\uparrow$ ) and where lower values mean better performance metrics are marked with ( $\downarrow$ ).

We choose four DNN models in this work to scrutinize their ability on our custom classification task. Generally we want to test and analyze a range of different architectures, but also compare models previously mentioned in the literature in this context. Our end goal is to identify the DNN architecture that can perform our target task of eelgrass detection with the highest accuracy. The ResNet models are well-known in their performance capabilities in image classification (Tan et al., 2018). InceptionNetV3 is mentioned previously in the literature (Reus et al., 2018) and its common use in image classification tasks. DenseNet architecture models show high accuracy in other image classification contexts, such as medical imaging (Kim et al., 2022), and efficiency in training time compared to ResNet architectures. Finally we choose the Vision Transformer

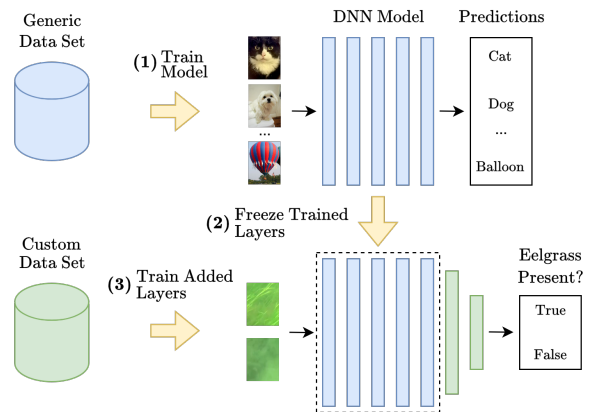


Fig. 5: Transfer learning: (1) we use DNN models pre-trained on a generic data set, here ImageNet (Russakovsky et al., 2015). The trained layers of each DNN model are frozen and infused into our custom training process (2). We fine-tune a small number of additional layers on our eelgrass data set to perform the target task of eelgrass detection (3).

model (configuration ViT\_l\_32) because they are considered state-of-the-art in image classification. We believe we are the first to apply ViTs in the context of eelgrass classification.

One fundamental challenge in assessing underwater image data is the light attenuation in water. To mitigate these factors and to increase visual quality of the images, we employ a DNN-based underwater (UW) image enhancement tool called DeepWave-Net (Sharma et al., 2023). We are curious whether this could have a positive effect on prediction accuracy of our DNN models because the images of ImageNet are predominantly taken on land, and thus do not exhibit above-mentioned shortcomings. We conduct all model training and testing procedures with and without the application of UW-enhancement (see Figure 6). The UW-enhanced images show a wider range of colors, a better contrast between the green and red channels on the RGB color range. This enables easier differentiation between the green/brown filamentous algae from the eelgrass itself, as well as the sugar kelp within the image. Furthermore, when applying the model on images at a greater water depth, we notice that the effect is even more significant.

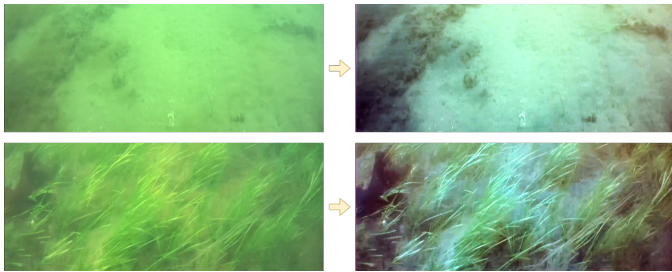


Fig. 6: Two images before (left) and after (right) applying underwater image enhancement.

To evaluate each model architecture, we run multiple machine learning experiments. To gauge baseline performance of each model architecture, we complete an initial experiment. Here we choose to use LYT-20 as a test dataset, due to its frequent changing underwater landscape, caused by its zig-zag constellation (see Fig. 2d). For training, we use all other transects, except LYT-9. LYT-9 is excluded since it is used as the final test dataset, and must be excluded for all experiments. For these experiments we create the validation dataset by using a random split of a 20% subset of images from the train dataset. The DNN classification layer configuration for the initial run (last layer and second last layer size) are configured as seen in Tbl. III. For these runs we choose to configure the second last layer with more neurons than the last layer to guide the learning process towards a natural dimensionality reduction.

After completion of the initial evaluation experiments, we choose a subset of models which performed best, and complete a cross-validation test. To overcome the challenge of imbalances in class distributions between different transects we devise an alternative approach to cross validation compared to traditional k-fold cross validation. We call this leave-one-transect-out cross validation. This approach only uses data from transects LYT-10, LYT-12 and LYT-20 due to their similar class distributions. On each cross validation fold we choose one of the three transects as the validation set, and the model trained on all other transects. We repeat this process of selecting one transect for validation three times, as such allowing for training and testing across all three transects. Upon completion we average the validation scores taken from all three experiments. This gives a good estimation of model performance, which is not directly overfit to one specific train and test dataset. The hyperparameters chosen for these experiments are the same as the hyperparameters used in initial experiments. Finally, based on the “leave-one-transect-out” validation test results, we select the two highest performing models and complete the final model experiment. This involves using all transects except LYT-9 as the train/validation dataset and test on the LYT-9 transect.

### F. Eelgrass Coverage Estimation and Postprocessing

In a traditional eelgrass transect methodology eelgrass coverage is defined by having marine biologists annotate how much of the observed area is covered in eelgrass as a percentage. In Denmark eelgrass coverage is defined as “the total substrate-

Model	Last Layer	Second To Last Layer	#Trainable Weights	#Frozen Weights	Learning Rate
ResNet	512	512	131K	11.4M	1.7e-05
InceptionNetV3	256	512	1.2M	25.1M	1.7e-05
DenseNet	256	512	623K	18.1M	1.7e-05
ViT	256	512	513K	306M	1.7e-05

TABLE III: Model Hyperparameters: For each chosen model architecture we report the size of the two additional layers (last and second to last layer) to be fine-tuned by transfer learning, the number of trainable weights for fine-tuning, the number of frozen weights and the learning rate.

specific coverage (determined) by projecting the outline of the foliage vertically onto the surface of the soft bottom and assessing the foliage’s percentage coverage of the bottom.” - translated from Danish (Bruhn et al., 2013). We find that this definition is unpractical to comply with when considering EIA video transects, where images are taken at an angle towards the seafloor. Alternatives such as visual coverage guides are highly subjective; the difference for example between 30% and 55% is extremely hard to determine (Short et al., 2015).

In this work we propose steps towards a novel, data-driven method for estimating eelgrass coverage. We are interested in developing a coverage estimation method that is based on the frequencies of outputs of the sample-based binary presence predictions of an image stream containing varying levels of eelgrass abundance. Since we consider spatially overlapping frames, we estimate the area with eelgrass present along the transect by calculating the temporal mean of the image stream with 0% representing eelgrass absent and 100% representing eelgrass present. The general expression of the temporal mean (TM) in a sequence of predictions  $p$  in a range  $r$  at instance  $i$  is given by:

$$TM_{r,i} = \frac{p_i + p_{i+1} + p_{i+2} + \dots + p_{i+r-1}}{r} = \frac{1}{r} \sum_{n=0}^{r-1} p_{i+n}. \quad (1)$$

We calculate the eelgrass coverage estimate with a range of  $r = 30$  samples, or 10 seconds of video footage. We deduce this rolling mean window size from the ship speed; assuming that the survey vessel sails at an average speed of around 1 m/s and each image contains around  $1m^2$  area, then 10s of footage gives a spatial area of around  $10m^2$ .

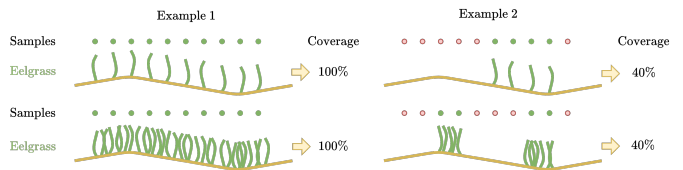


Fig. 7: Limitations: even though the level of eelgrass abundance is different in the top scenes compared to the bottom scenes, eelgrass coverage estimation based on a temporal mean of ten samples gives the same result in both examples.

We argue that this method can give an estimate of visual eelgrass coverage. For example, if there is a high frequency of con-

secutive frames with eelgrass present, then this denotes the presence of a consistent eelgrass coverage. If the frequency is low, then eelgrass becomes more patchy, and less frequent, denoting a lower eelgrass coverage. Our method has several advantages: (1) it is highly automated, scalable and practical once a suitable classifier is trained, (2) it can potentially predict eelgrass coverage in real-time and thus improve EIA transects monitoring even during their execution, (3) it is potentially less biased than human labeling and thus more reliable and repeatable.

There are some limitations to our coverage estimation method as depicted in Fig. 7. First, consecutive images that have consistently little eelgrass present give the same coverage estimation as consecutive images with abundant eelgrass (example 1). Therefore, there is no distinction in the abundance as such, since the frequency of images with the binary prediction “eelgrass present” is the same. Second, it is not possible to determine the location of small and dense eelgrass patches as they give the same coverage estimation as larger sparse patches. The temporal mean obliterates this information (example 2). Third, the method is sensitive to the temporal mean window size. Even though these limitation exist we argue that they are outweighed by the advantages of our method mentioned above.

To extract the overlaid positional meta-data from the transect videos we use the Tesseract Engine (Smith, 2007) for optical character recognition. We fuse the resulting GPS data with our eelgrass annotations and DNN-based predictions. We choose transects LYT-9, LYT-10, LYT-11, LYT-12, LYT-13, LYT-19 and LYT-20. For each transect, we use our ViT model to get a prediction for every 10th frame. Since all the videos are filmed at 30 frames per second, this gives three predictions per second. In total this creates 16796 predictions of eelgrass presence, related to a geographical position along each of the transects. To further give intuition on the benefits of our novel estimation coverage approach we conduct a visual comparison between our approach and human annotations on a transect video from an EIA in a different location in Denmark (around 150km away), since we have annotated coverage estimations available for this specific video transect. We cut a 15 minute section (around 900m to 1350m) from this transect and use our ViT predictions to estimate coverage.

### III. RESULTS

#### A. Initial Model Evaluation

The results of our initial model evaluation experiments are shown in Tbl. IV. Based on the high level of AUROC scores, and a low variation for all models, we ascertain that the task of eelgrass classification can in fact be conducted by DNN models. Secondly, the models trained and tested on UW-enhanced images show a higher accuracy compared to their non-enhanced counterparts in 26/30 cases. Thus UW-enhancement has a positive effect the models’ ability to predict eelgrass presence accurately in the context of transfer learning with pre-training on Imagenet. We conclude that some models may benefit from UW-image enhancement. Generally we find that the Vision Transformer and DenseNet architecture show good performance on the target task. Surprisingly the

smallest ResNet model, ResNet-18++, gives the best results across all three metrics among the ResNet models. The Vision Transformer shows the best results overall compared to all DNN architectures across all three metrics.

We are interested in how the test calibration error changes between the top AUROC performing models. This highlights that different models are over/under-confident during prediction. For example DenseNet-169++ and InceptionNetV3++, which both have equal AUROC scores, however DenseNet-169++ has a higher test calibration error than InceptionNetV3++. We conclude that InceptionNetV3 is a more stable model, and not as prone as to over/under-predicting the posterior probabilities compared to the DenseNet model.

TABLE IV: Test results from initial experiments, with models trained on LYT-5, LYT-10, LYT-12 and LYT-14 and tested on LYT-20. The 3 metrics of interest are test accuracy, are under ROC curve (AUROC) and test calibration error (CE). Higher scores mean better performance and are marked by (↑) and vice versa marked by (↓). Models trained and tested on UW-enhanced images are marked by ++.

Model	Accuracy (↑)	AUROC (↑)	CE(↓)
ResNet-18	0.769	0.892	0.203
ResNet-18++	<b>0.792</b>	<b>0.902</b>	<b>0.188</b>
ResNet-34	0.730	0.877	0.252
ResNet-34++	0.777	0.876	0.215
ResNet-50	0.784	0.895	0.191
ResNet-50++	0.766	0.894	0.222
ResNet-101	0.767	0.887	0.211
ResNet-101++	0.782	0.892	0.197
ResNet-152	0.748	0.886	0.229
ResNet-152++	0.761	0.895	0.220
InceptionNetV3	0.794	0.893	0.184
InceptionNetV3++	<b>0.828</b>	<b>0.909</b>	<b>0.155</b>
DenseNet-121	0.779	0.899	0.213
DenseNet-121++	0.813	<b>0.914</b>	0.176
DenseNet-169	0.788	0.902	0.208
DenseNet-169++	0.826	0.908	0.160
DenseNet-201	0.818	0.907	0.169
DenseNet-201++	<b>0.835</b>	<b>0.914</b>	<b>0.156</b>
ViT	0.830	0.914	0.161
ViT++	<b>0.867</b>	<b>0.938</b>	<b>0.125</b>

#### B. Leave-One-Transect-Out Results

As can be seen in Tbl. V, the ViT architecture continuously shows the best performance, with the enhanced version ViT++ performing best. Using models on UW-enhanced data also continues to provide the highest model scores across all model architectures. We also notice that the smaller DenseNet-169++ model has a higher accuracy than the DenseNet-201, although performing worse in the AUROC and CE categories. This highlights the importance of using multiple different metrics to evaluate models.

#### C. Final Test Dataset Model Results

We report our final model test results in Tbl. VI. In the final model training and testing, for non-enhanced models both DenseNet-201 and Vision Transformer achieve high scores, with both models gaining high AUROC scores on the test set. Both models also achieved very low calibration error



TABLE V: Leave-one-transect-out cross validation results. The 3 metrics of interest are test accuracy, area under ROC curve (AUROC) and test calibration error (CE). Higher scores mean better performance and are marked by ( $\uparrow$ ) and vice versa marked by ( $\downarrow$ ). Models trained and tested on UW-enhanced images are marked by ++.

Model	Accuracy ( $\uparrow$ )	AUROC ( $\uparrow$ )	CE ( $\downarrow$ )
ResNet-18	<b>0.870</b>	<b>0.939</b>	0.098
ResNet-18++	0.867	0.936	<b>0.097</b>
InceptionNetV3	0.855	0.936	0.115
InceptionNetV3++	<b>0.868</b>	<b>0.940</b>	<b>0.108</b>
DenseNet-169	0.866	0.942	0.105
DenseNet-169++	<b>0.879</b>	0.943	0.099
DenseNet-201	0.874	0.944	0.105
DenseNet-201++	0.875	<b>0.946</b>	<b>0.095</b>
ViT	0.852	0.938	0.126
ViT++	<b>0.901</b>	<b>0.953</b>	<b>0.082</b>

scores, 0.084 and 0.086 respectively, showing both models capability to not only predict accurately, but also confidently. Overall the Vision Transformer performed best across all metrics. Both models showed an increase in performance when trained and tested on the UW-enhanced images. With a total training time of around 30 minutes we show that our transfer learning approach is highly efficient, compared to training a ViT from scratch which can take up to three days on four GPUs (Touvron et al., 2021).

TABLE VI: Final Model Results: Models trained and tested on enhanced images are marked by ++.

Model	Accuracy ( $\uparrow$ )	AUROC ( $\uparrow$ )	CE ( $\downarrow$ )	Train Time ( $\downarrow$ )
DenseNet-201	0.877	<b>0.955</b>	0.113	30min
DenseNet-201++	<b>0.878</b>	<b>0.955</b>	<b>0.110</b>	30min
ViT	0.877	0.955	0.113	28min
ViT++	<b>0.902</b>	<b>0.959</b>	<b>0.087</b>	28min

#### D. Eelgrass Presence and Coverage Estimation

We map the ViT predictions from LYT-9, LYT-10, LYT-11, LYT-13, LYT-19, LYT-20 geographically in Fig. 8a. The green marks denoting the presence of eelgrass, and yellow the absence. In Fig. 8b all eelgrass present data points are mapped on a heat map, giving us a good visual estimation for eelgrass coverage in the area. We also present information on the extracted eelgrass distribution relative to water depth. This relationship is plotted relative to a normalized water depth bin, since the water depth data is not equally distributed (see Fig. 9).

Since we do not have expert labels on eelgrass coverage available of the LYT transects, we show how our coverage estimation compares with manual labels of a different EIA transect video. In Fig. 10 we show the eelgrass coverage estimation based on our ViT predictions compared to video analysis labeled by experts. The respective transect video was taken at a location around 150km away from the LYT video transects. We can see that our estimation based on temporal means of ViT predictions shows spikes in similar timestamps compared to the expert labels. Figure 10 demonstrates that our

method is generalizable to an environment with a significantly different seabed.

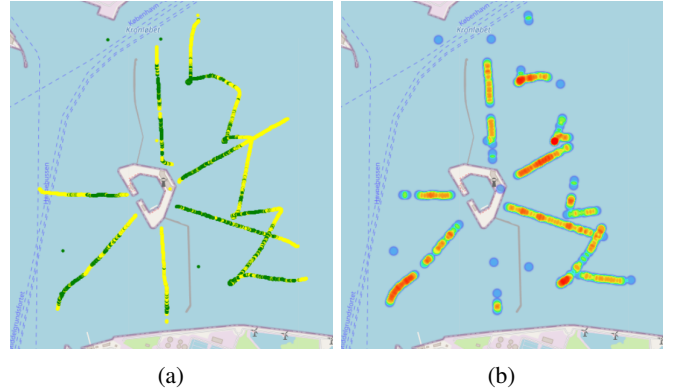


Fig. 8: (a) Eelgrass presence: the lines mark transect surveys conducted in the Copenhagen harbor along planned survey paths, green dots indicate detected eelgrass presence along each transect, yellow dots indicate eelgrass absence. (b) Eelgrass coverage: an estimation of eelgrass coverage in the benthic environment represented by a heat map of the transects.

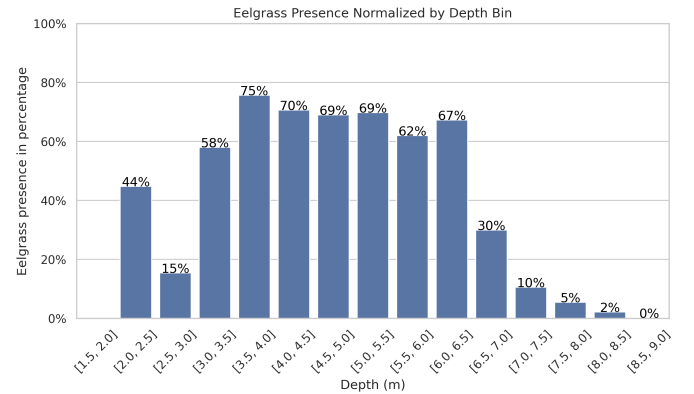


Fig. 9: Eelgrass presence percentage categorized by depth (m).

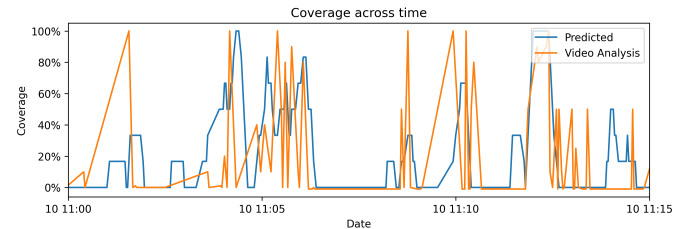


Fig. 10: Visual Coverage Estimation: (blue) our new approach based on the temporal mean of ViT predictions of a transect video, (orange) human annotated eelgrass coverage values.

## IV. DISCUSSION

### A. Video Data Limitations and Solutions

During the sailing of the transect surveys, the recorded video footage is streamed to video processing software which adds GPS location, water depth and heading (i.e. course over ground measured in degrees) to each video as an overlay. Streaming lag

can cause a delay in the timestamps in the imprinted overlay. This is problematic when trying to align the images to GPS locations during post-processing. Additionally there is a mismatch ( $\sim 5\text{-}20\text{m}$ ) between the imprinted GPS locations of the vessel and the actual camera position on the towed sled. One approach to improve GPS position accuracy, and generally make steps towards automated eelgrass inspection is to deploy Autonomous Underwater Vehicles (AUVs). AUVs have multiple benefits, for example more accurate position estimation compared to a towed sled, which can be achieved by fusing information from additional location sensors. This work is directly applicable to a scenario where an AUV with a forward-facing camera is deployed to autonomously perform EIAs without a manual operator. The AUV might have a high-level objective of inspecting seagrass meadows and therefore needs to detect the meadow boundaries in real-time, as for example demonstrated by Ruscio et al. (Ruscio et al., 2023). With our analysis on DNN performance, a robotics engineer can choose a suitable model according to hardware constraints for integration into the AUV navigation stack.

Finally, during inspection of some of the transect images, we noticed motion blur in some frames. This was initially attributed to the camera’s low quality and frame-rate and later suspected to stem from an automated video compression. To overcome this we recommend investing in a high-quality waterproof camera system. It is important to mention that humans are good at filtering out such motion trails, while DNN models are not, due to their dependence on raw pixel data. Therefore this should be taken into consideration when using this dataset for future applications.

### B. Eelgrass Coverage Estimation

In this work, we present a novel idea for eelgrass coverage estimation to overcome practical constraints of traditional methods. We outline the benefits and limitations of our approach in Sect. II-F. Additionally we argue, that human labeling inherently suffers from observer bias. Although DNNs are not immune to biases, they can reduce variability across images and perspectives as well as offer a consistent and deterministic analytical process, once they are trained. Human labeling also suffers from the tendency of annotators to focus disproportionately on specific parts of an image. This issue is particularly pronounced here since our images are captured at an angle towards the seafloor; eelgrass in the foreground might induce the annotator to indicate a high coverage percentage even if there is little eelgrass present in the background. We assert that our data-driven approach of calculating the temporal mean of our DNN-based binary predictions offers a robust and accurate approach to estimating eelgrass coverage in the wild. Here we would like to stress that this approach should act as a supportive tool for marine biologists to conduct EIAs in a more data-driven manner. This tools presented in this work should not be seen as a replacement for expert domain knowledge, rather, a showcase to apply state-of-the-art technologies to support marine experts in their work.

### C. Underwater Image Enhancement

We find that applying Deep WaveNet (Sharma et al., 2023) as an UW image enhancement tool proves to be effective in improving model accuracy. However, the computational demands are substantial, requiring approximately three hours of processing time on an A10G GPU for the entire training set, or around 1.2 seconds per image. The trade-off between the computational investment and the incremental performance gains must be carefully considered in practice, given the rising carbon footprint of training of DNNs (Luccioni and Hernandez-Garcia, 2023). Additionally, it is also important to consider the potential for the the Deep WaveNet model to introduce bias in eelgrass presence classification based on water depth. As Sharma et al. show, the receptive field size of global features is more effective at greater water depths, than in shallow waters. Since all transects used for model training and testing occur in water depths of 2-14m, the impact of Deep WaveNet in this context is minimal but cannot be entirely discounted.

## V. CONCLUSION

This work shows the potential of deep learning models to automate the process of seagrass detection in underwater video transects from challenging visual conditions in the wild. By training a deep neural networks to classify underwater images into “Eelgrass Present” and “Eelgrass Absent” classes, our proposed methodology allows for the efficient processing of large volumes of video data collected in environmental impact assessments, enabling the acquisition of much more detailed information on seagrass distributions compared to current manual annotation methods. Our results show that deep learning models, particularly Vision Transformers, can achieve high performance in predicting eelgrass presence, with AUROC scores exceeding 0.95 on the final test dataset. We also show an effective implementation of transfer learning, and that the application of the underwater image enhancement model further improves model’s capabilities.

Beyond the technical aspects, we also propose a methodology which combines existing data acquisition methods like video transects with a streamlined annotation platform, as well as advancements in the field of machine learning. We highlight how such a methodology has significant benefits, including faster and more accurate data annotation, the potential for automated quality assurance and long term automation benefits. We emphasize that deep neural networks are positioned as supportive tools to augment the work of marine biologists. Broadly we prospect that this work serves as a framework for a marine imaging workflow which can be implemented on other underwater flora.

Overall, this project demonstrates the value that deep learning can bring to the field of marine ecology and environmental monitoring. By automating the processing of underwater video data, it opens up new possibilities for gaining a deeper understanding of seagrass ecosystems and their response to environmental changes. As the human impacts on seagrass beds continue to increase worldwide, tools like the one we propose, will become increasingly important for effective conservation and management efforts.

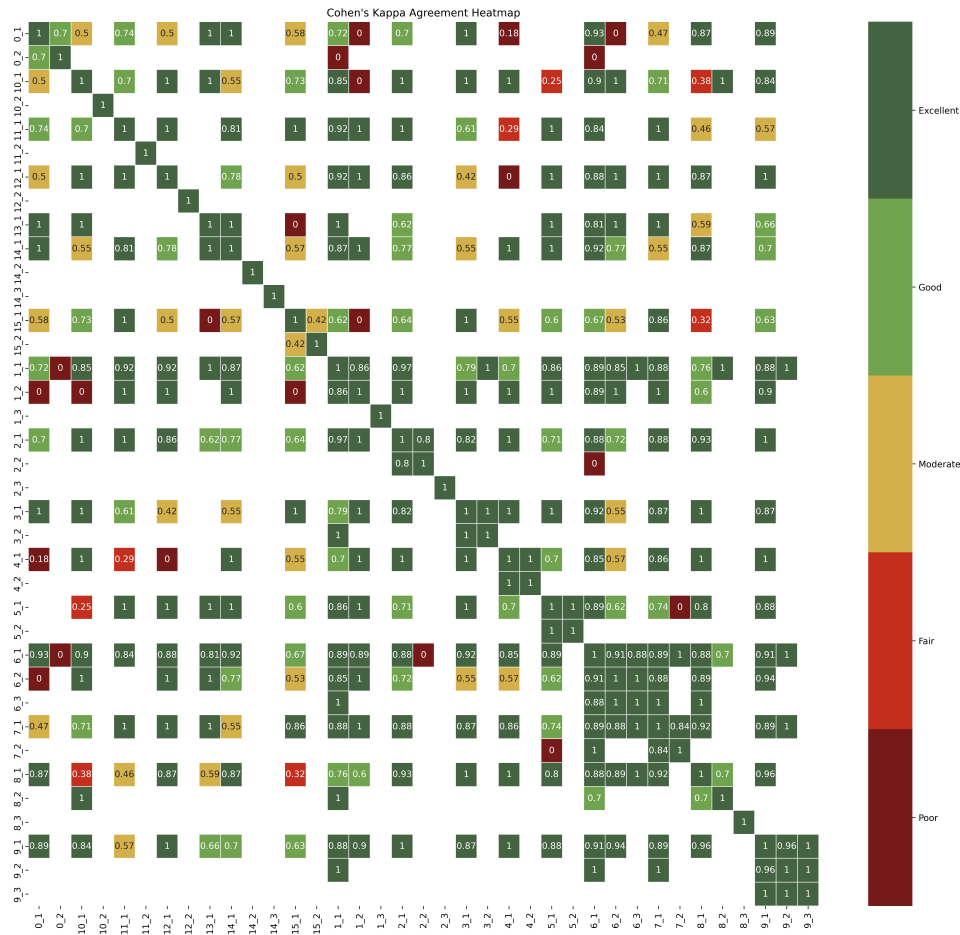


Fig. 11: Cohens kappa scores for all annotators

## VI. ACKNOWLEDGMENTS

The authors would like to thank their collaborators at DHI: Aron Lank Jensen, Jesper Goodley Dannisøe and Lindsey Aies. This project was funded and run in collaboration with DHI (DHI, 2023). This project has received funding from the European Union’s Horizon 2020 research and innovation programme under the Marie Skłodowska-Curie grant agreement No 956200.

## APPENDIX

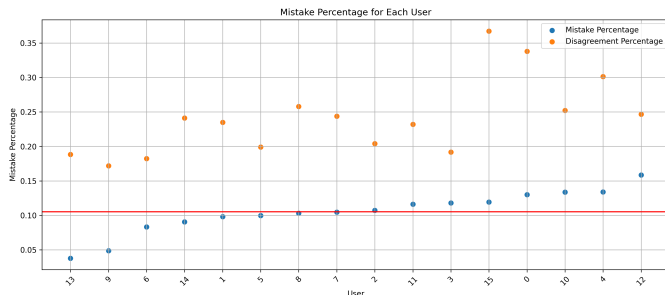


Fig. 12: Mistakes percentage and disagreement percentage for each annotator.

## REFERENCES

- Annette Bruhn, Signe Høgslund, Karsten Dahl, Dorte Krause-Jensen, and Michael Bo Rasmussen. AU Ecoscience - Marint fagdatacenters gældende tekniske anvisninger, 2013. URL <https://ecos.au.dk/forskningraadgivning/fagdatacentre/marint-fagdatacenter/gaeldende-tekniske-anvisninger>. Accessed: 2024-12-9.
- Leanne C Cullen-Unsworth, Lina Mtwana Nordlund, Jessica Paddock, Susan Baker, Len J McKenzie, and Richard KF Unsworth. Seagrass meadows globally as a coupled social-ecological system: Implications for human wellbeing. *Marine pollution bulletin*, 83(2):387–397, 2014.
- DHI. Dhi - we enable a sustainable future for water, October 2023. URL <https://www.dhigroup.com>. Publication Title: DHI.
- Alexey Dosovitskiy. An image is worth 16x16 words: Transformers for image recognition at scale. *arXiv preprint arXiv:2010.11929*, 2020.
- Charles W Finkl and Christopher Makowski. *Seafloor Mapping Along Continental Shelves: Research and Techniques for Visualizing Benthic Environments*, volume 13. Springer, 2016.

- James W Fourqurean, Carlos M Duarte, Hilary Kennedy, Núria Marbà, Marianne Holmer, Miguel Angel Mateo, Eugenia T Apostolaki, Gary A Kendrick, Dorte Krause-Jensen, Karen J McGlathery, et al. Seagrass ecosystems as a globally significant carbon stock. *Nature geoscience*, 5(7):505–509, 2012.
- Brian Fry and Patrick L Parker. Animal diet in texas seagrass meadows:  $\delta^{13}C$  evidence for the importance of benthic plants. *Estuarine and Coastal Marine Science*, 8(6):499–509, 1979.
- Mustafa Umit Gumusay, Tolga Bakirman, Inci Tuney Kizilkaya, and Nedim Onur Aykut. A review of seagrass detection, mapping and monitoring applications using acoustic systems. *European Journal of Remote Sensing*, 52(1):1–29, 2019.
- Kaiming He, Xiangyu Zhang, Shaoqing Ren, and Jian Sun. Deep residual learning for image recognition. In *Proceedings of the IEEE conference on computer vision and pattern recognition*, pages 770–778, 2016.
- Marten A Hemminga and Carlos M Duarte. *Seagrass ecology*. Cambridge University Press, 2000.
- Gao Huang, Zhuang Liu, Laurens Van Der Maaten, and Kilian Q Weinberger. Densely connected convolutional networks. In *Proceedings of the IEEE conference on computer vision and pattern recognition*, pages 4700–4708, 2017.
- Hee E Kim, Alejandro Cosa-Linan, Nandhini Santhanam, Mahboubeh Jannesari, Mate E Maros, and Thomas Ganslandt. Transfer learning for medical image classification: a literature review. *BMC medical imaging*, 22(1):69, 2022.
- Alex Krizhevsky, Ilya Sutskever, and Geoffrey E Hinton. Imagenet classification with deep convolutional neural networks. *Advances in neural information processing systems*, 25, 2012.
- Ananya Kumar, Percy S Liang, and Tengyu Ma. Verified uncertainty calibration. *Advances in Neural Information Processing Systems*, 32, 2019.
- JR Landis. The measurement of observer agreement for categorical data. *Biometrics*, 1977.
- Alexandra Sasha Luccioni and Alex Hernandez-Garcia. Counting carbon: A survey of factors influencing the emissions of machine learning. *arXiv preprint arXiv:2302.08476*, 2023.
- Lena Maier-Hein, Annika Reinke, Patrick Godau, Minu D Tizabi, Florian Buettner, Evangelia Christodoulou, Ben Glocker, Fabian Isensee, Jens Kleesiek, Michal Kozubek, et al. Metrics reloaded: recommendations for image analysis validation. *Nature methods*, 21(2):195–212, 2024.
- Md Moniruzzaman, Syed Mohammed Shamsul Islam, Paul Lavery, and Mohammed Bennamoun. Faster r-cnn based deep learning for seagrass detection from underwater digital images. In *2019 digital image computing: techniques and applications (DICTA)*, pages 1–7. IEEE, 2019.
- Md Kislunoman, Syed Mohammed Shamsul Islam, Jumana Abu-Khalaf, Seyed Mohammad Jafar Jalali, and Paul Lavery. Improving accuracy and efficiency in seagrass detection using state-of-the-art ai techniques. *Ecological Informatics*, 76:102047, 2023.
- Alyssa B Novak and Frederick T Short. Submerged aquatic vegetation: seagrasses. In *Coastal and Marine Environments*, pages 277–288. CRC Press, 2020.
- Robert J Orth, Tim JB Carruthers, William C Dennison, Carlos M Duarte, James W Fourqurean, Kenneth L Heck, A Randall Hughes, Gary A Kendrick, W Judson Kenworthy, Suzanne Olyarnik, et al. A global crisis for seagrass ecosystems. *Bioscience*, 56(12):987–996, 2006.
- Adam Paszke, Sam Gross, Francisco Massa, Adam Lerer, James Bradbury, Gregory Chanan, Trevor Killeen, Zeming Lin, Natalia Gimelshein, Luca Antiga, et al. Pytorch: An imperative style, high-performance deep learning library. *Advances in neural information processing systems*, 32, 2019.
- Scarlett Raine, Ross Marchant, Peyman Moghadam, Frederic Maire, Brett Kettle, and Brano Kusy. Multi-species seagrass detection and classification from underwater images. In *2020 Digital Image Computing: Techniques and Applications (DICTA)*, pages 1–8. IEEE, 2020.
- Gereon Reus, Thomas Möller, Jonas Jäger, Stewart T Schultz, Claudia Kruschel, Julian Hasenauer, Viviane Wolff, and Klaus Fricke-Neudert. Looking for seagrass: Deep learning for visual coverage estimation. In *2018 OCEANS-MTS/IEEE Kobe Techno-Oceans (OTO)*, pages 1–6. IEEE, 2018.
- Bernhard M Riegl and Samuel J Purkis. Detection of shallow subtidal corals from ikonos satellite and qtc view (50, 200 khz) single-beam sonar data (arabian gulf; dubai, uae). *Remote Sensing of Environment*, 95(1):96–114, 2005.
- Chris M Roelfsema, Eva M Kovacs, and Stuart R Phinn. Field data sets for seagrass biophysical properties for the eastern banks, moreton bay, australia, 2004–2014. *Scientific Data*, 2(1):1–6, 2015.
- Francesco Ruscio, Riccardo Costanzi, Nuno Gracias, Josep Quintana, and Rafael Garcia. Autonomous boundary inspection of posidonia oceanica meadows using an underwater robot. *Ocean Engineering*, 283:114988, 2023.
- Olga Russakovsky, Jia Deng, Hao Su, Jonathan Krause, Sanjeev Satheesh, Sean Ma, Zhiheng Huang, Andrej Karpathy, Aditya Khosla, Michael Bernstein, et al. Imagenet large scale visual recognition challenge. *International journal of computer vision*, 115:211–252, 2015.
- Sayantana Sengupta, Bjarne Kjær Ersbøll, and Anders Stockmarr. Seagrassdetect: A novel method for the detection of seagrass from unlabelled underwater videos. *Ecological Informatics*, 57:101083, 2020.
- Prasen Sharma, Ira Bisht, and Arijit Sur. Wavelength-based attributed deep neural network for underwater image restoration. *ACM Transactions on Multimedia Computing, Communications and Applications*, 19(1):1–23, 2023.
- Frederick T Short and Robert G Coles. *Global seagrass research methods*. Elsevier, 2001.
- Frederick T Short, Robert G Coles, and CA Short. Seagrassnet manual for scientific monitoring of seagrass habitat. 2015.
- Ray Smith. An overview of the tesseract ocr engine. In *Ninth international conference on document analysis and recognition (ICDAR 2007)*, volume 2, pages 629–633. IEEE, 2007.
- Christian Szegedy, Vincent Vanhoucke, Sergey Ioffe, Jon Shlens, and Zbigniew Wojna. Rethinking the inception



- architecture for computer vision. In *Proceedings of the IEEE conference on computer vision and pattern recognition*, pages 2818–2826, 2016.
- Chuanqi Tan, Fuchun Sun, Tao Kong, Wenchang Zhang, Chao Yang, and Chunfang Liu. A survey on deep transfer learning. In *Artificial Neural Networks and Machine Learning–ICANN 2018: 27th International Conference on Artificial Neural Networks, Rhodes, Greece, October 4-7, 2018, Proceedings, Part III* 27, pages 270–279. Springer, 2018.
- Jorge Terrados and Carlos M Duarte. Experimental evidence of reduced particle resuspension within a seagrass (*Posidonia oceanica* L.) meadow. *Journal of experimental marine biology and ecology*, 243(1):45–53, 2000.
- Hugo Touvron, Matthieu Cord, Matthijs Douze, Francisco Massa, Alexandre Sablayrolles, and Hervé Jégou. Training data-efficient image transformers & distillation through attention. In *International conference on machine learning*, pages 10347–10357. PMLR, 2021.
- Richard KF Unsworth, Len J McKenzie, Catherine J Collier, Leanne C Cullen-Unsworth, Carlos M Duarte, Johan S Eklöf, Jessie C Jarvis, Benjamin L Jones, and Lina M Nordlund. Global challenges for seagrass conservation. *Ambio*, 48: 801–815, 2019.
- Bijeesh Kozhikkodan Veetil, Raymond D Ward, Mariana Do Amaral Camara Lima, Milica Stankovic, Pham Ngoc Hoai, and Ngo Xuan Quang. Opportunities for seagrass research derived from remote sensing: A review of current methods. *Ecological Indicators*, 117:106560, 2020.
- Jiangtao Wang, Baihua Li, Yang Zhou, Qinggang Meng, Sante Francesco Rende, and Emanuele Rocco. Real-time and embedded compact deep neural networks for seagrass monitoring. In *2020 IEEE International Conference on Systems, Man, and Cybernetics (SMC)*, pages 3570–3575. IEEE, 2020.
- Michelle Waycott, Carlos M Duarte, Tim JB Carruthers, Robert J Orth, William C Dennison, Suzanne Olyarnik, Ainsley Calladine, James W Fourqurean, Kenneth L Heck Jr, A Randall Hughes, et al. Accelerating loss of seagrasses across the globe threatens coastal ecosystems. *Proceedings of the national academy of sciences*, 106(30):12377–12381, 2009.